Pergamon

NanoStructured Materials, Vol. 5, No. 3, pp.363-372, 1995

0965-9773/95 $9.50 + .00

0965-9773(95)00238-3

CdS NANOCRYSTALS EMBEDDED IN SILICA SONOGEL

A. Craievich
Laboratorio Nacional de Luz Sincrotron/CNPq. CP. 6192, 13081, Campinas
and Institute of Physics/USP, Sao Paulo, Brazil

N. de la Rosa-Fox, E. Blanco, M. Piñero, M. Ramirez-del-Solar and L. Esquivias
Dpto. de Fisica de la Materia Condensada (Grupo Geles)
Facultad de Ciencias, Universidad de Cadiz, Aptdo 40-11510-Puerto Real (Cadiz), Spain

(Accepted January 1995)

Abstract— *Monolithic silica gel was prepared combining sonochemistry and the use of a drying control chemical additive (DCCA); it was used as a host-matrix for a nanocomposite. CdS nanocrystals were precipitated by exposing the porous gel to H_2S gas. Transmission electron microscopy (TEM) and absorption X-ray (XANES- Cd K edge) experiments reveal the presence of CdO clusters as a consequence of an incomplete sulphurization inside the total matrix volume. The CdS crystal size was estimated to range from 3 to 5 nm by means of small angle X-ray scattering (SAXS), using the best Guinier region after mathematical data reduction. Optical absorption spectra confirm quantum confinement effects in CdS nanocrystals.*

INTRODUCTION

Sol-Gel processing provides materials with very interesting technological applications (1,2). In the particular case of silica, the chemical approach utilizes the hydrolysis and polycondensation reactions of a metallic alkoxide (tetraethylorthosilicate) to give the silica gel. At this step, before gelation, the manipulation at a molecular level can be controlled by means of several parameters, such as pH, temperature, concentration, liquid surface tension, chemical additives and time-temperature history. As a consequence, it is possible to change the main textural parameters that govern the porous network of gels, that is, average pore size, pore size distribution, pore volume fraction, specific surface area, bulk and skeletal densities. This structural manipulation can be made during the gelation, aging, drying and sintering processing steps, making it possible to tailor gels for specific practical applications (3).

When the sol-gel method is used to obtain a nanocomposite, the porous and dielectric nature of silica gel is the reason which makes this "coherent structure inside a fluid" an attractive material for optical purposes. Inside the porosity other compounds can be trapped, organic and/or inorganic, to produce a strong change in the physico-chemical properties of silica. Recently, the materials research community focused its attention on the semiconductor nanocrystals-doped gels, due to their high degree of optical non-linearity (4,5). The semiconductor nanocrystals, as a fine

dispersion inside the dielectric silica matrix, operate as quantum dots producing the confinement of discrete excitons, and lead to an optical response with intensity dependent refractive index (6). Moreover, silica has a wide band-gap energy and the confinement effect of embedded semiconductor nanoparticles is very large, operating as a true potential well.

The sol-gel processing for the preparation of semiconductor-doped gels has been used since chalcogenides can easily be prepared by chemical precipitation at room temperature (7). The study of the chemical parameters affecting the crystal nature and size distribution of nanocrystals has been the aim of many works in the past few years (8-11). Chalcogenides are often chosen because they have high values of third-order susceptibility and short switching times (12,13).

In order to obtain small crystals it is necessary to produce a great number of nucleation centers and a matrix with a fine porosity to prevent the subsequent crystal growth. Previous studies (14,15) have shown that the combined effect of the addition of formamide (DCCA) in the sol and the action of high power ultrasound to promote the chemical reactions, permits the tailoring of specific structures. This processing has been applied to obtain CdS-doped gels, taking advantage of their favorable features, homogeneous size distribution and fine porosity. In a recent study (15) it was shown that a fine dispersion of CdS nanocrystals can be formed in porous SiO_2 xerogels. The host-matrix was a xerogel prepared from a precursor mixture of TMOS (Tetramethoxysilane) and water using sonochemistry (instead of alcohol dilution) and formamide as a DCCA. The present work concerns a similar study of a set of composites prepared from solventless alkoxide-water mixtures using TEOS (Tetraethoxysilane) instead of TMOS, given the differences in their gelation kinetics.

EXPERIMENTAL PROCEDURE

The procedure of obtaining the CdS nanocrystal dispersion in porous SiO_2 gel was similar to that used in the previous investigation, where the matrix was a TMOS-based xerogel (15). The composition of the starting liquid mixture was: [TEOS, acidic water, formamide] in a molar ratio 1:10:7, this sample is a pure silica sonogel matrix (A). Cd^{+2} ions were added to the liquid from a $Cd(NO_3)_2$ water solution to obtain a silica sonogel with well-dispersed Cd^{+2} ions as a "white" sample (**W**). In all cases, the liquid reaction was promoted by the action of high power ultrasound (600 W nominal output), the energy dose employed was 280 J cm^{-3}.

After the gels had been left to age at room temperature, the $S^{=}$ ions were introduced by H_2S gas diffusion into the porous network of the gels, producing a nucleation of small CdS crystals or $CdO \rightarrow CdS$ conversion. H_2S gas diffusion was made either by using dry H_2S to obtain the sample (M) or in hermetically closed containers (10 x 7 x 3 mm) from the thermal decomposition of thioacetamide at 40°C, using in all cases 25% of the gel weight. From this last method two samples were obtained, a short time (4 h) H_2S diffused sample (**DS**- diffused short) and a long time (7 h) H_2S diffused sample (**DL**-diffused long). The cadmium molecular content corresponds to ~10 wt. % of the final CdS in the SiO_2 matrix when 100% of the CdS reacts, leading to a composite composition of $(CdS)_{10}$-$(SiO_2)_{90}$.

The final gels were stabilized by soaking the gel in the precursor sonosol having the same composition as the matrix sol under vacuum at room temperature. This method allows the superficial pores to be sealed, thus ensuring greater longevity (16,17) and good optical stability due to a decrease of the aging process rate (18).

STRUCTURAL CHARACTERIZATION

The structural characterization of the composite formed by the impregnated porous SiO_2 xerogel and precipitated nanoparticles was carried out using three techniques: Transmission Electron Microscopy (TEM), Small Angle X-ray Scattering (SAXS) and X-ray Absorption Near-Edge Spectroscopy (XANES). TEM provides an analysis in the real space and SAXS provides an analysis in the reciprocal space of the heterogeneities. XANES gives chemical information that may be connected with the bonding type of the absorbing atom, around Cd atoms in the present study.

TEM Micrographs

Transmission electron microscopy was carried out in the JEOL JEM1200 EX of the University of Cadiz facility. A TEM micrograph of the xerogel before H_2S diffusion is shown in Figure 1a. This is called a "white" sample (**W**) because it does not have the characteristic yellow color of those in which H_2S has been diffused. The micrograph shows a grain of xerogel formed by a matrix containing nearly spherical particles with sizes ranging from about 2 up to 10 nm. The matrix in which these particles are immersed exhibits ill-defined, less-absorbent heterogeneities corresponding to the host xerogel porosity. The particles observed as darker spots by TEM absorb the electrons more strongly than the matrix, suggesting that they are formed by aggregation of Cd in CdO nanoparticles, as was also observed in the previous study on xerogels prepared from a TMOS precursor (11). In the TEM picture, the structural features of the porosity are not clear, but the existence of approximately isometric CdO nanocrystals is apparent.

Figure 1 b shows a TEM micrograph of **DS** sample, where nanocrystals are seen as darker spots, approximately the same size and distribution as **W** sample, keeping in mind the difference in the micrograph magnification. In this sample many of them have converted into CdS, because the samples have the characteristic yellow color and band absorption in the visible region (Figure 5, see below). In both cases of **W** and **DS** samples, the electron diffraction on a selected area gives reflections that correspond to the cubic-CdO and hexagonal-CdS crystalline phases, respectively.

XANES Spectra

The XANES measurements were performed using the DCI synchrotron radiation source at LURE (Orsay, France). The XANES spectra in the Cd K edge for samples **W** and **M**, shown in Figure 2 reveal several features. The curves show a small shoulder (labeled **a**) for both samples due to internal transitions between electronic states independent of the local Cd symmetry, since it is found at the same energy in every sample (26615 ± 5 eV from the edge threshold). Generally, this type of feature for such low energy photoelectrons, characteristic of electronic transitions to unoccupied high-energy states near the Fermi level, is sensitive to the local geometry of the absorber atom. This is enhanced by six-fold coordination as it is also present in the XANES spectra of CdS, and much more of the CdO commercial powdered crystals used as reference.

Another type of information can be obtained from a shape analysis. The edge width is related to the absorber symmetry as it defines the splitting of the degenerate energy levels and, therefore, the edge width should be small for highly symmetric coordination. The edge width is narrower and the oscillation amplitudes are higher in the CdO and **W** samples than CdS and **M** samples.

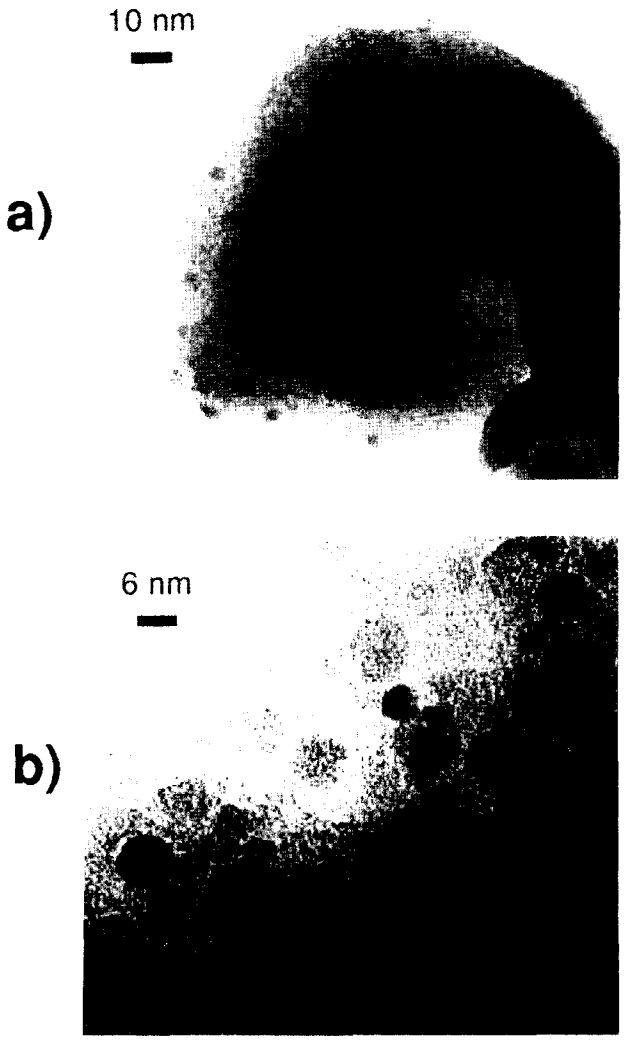

Figure 1 (a) TEM micrograph of the **W** sample. CdO nanocrystals can be seen as darker spots, ranging from 3-10 nm in size (before H_2S gas diffusion); and (b) TEM micrograph of the **DS** sample. After H_2S gas diffusion the CdS nanocrystals are also visible as darker spots.

These features are commonly associated with a more ionic character of the probe atom that corresponds to a higher coordination number of Cd in the pure cadmium sulfide ($N_{cn} = 6$) than in pure cadmium oxide ($N_{cn} = 4$). There is an edge shift of ~ 20 eV between the CdO and CdS spectra. This is in agreement with a degree of covalency change between these two compounds. The spectrum threshold of the sample under investigation (curve **M**) is found between those of the reference bulk materials (CdO and CdS), indicating that its covalent nature is intermediate between CdO and CdS, or rather **W**. This last spectrum is shifted ~10 eV toward higher energy relative to the CdO threshold probably due to the small size of the nanocrystals.

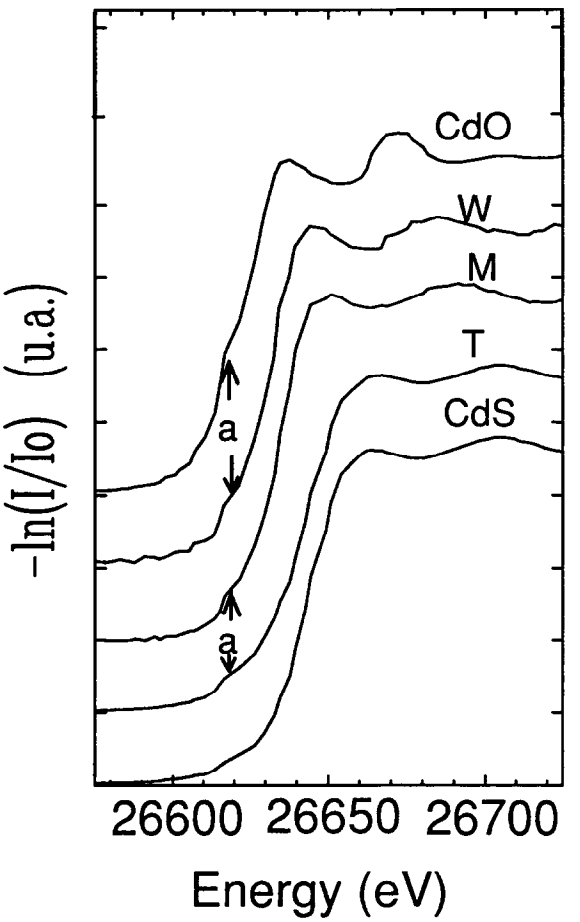

Figure 2. XANES spectra of **W** and **M** samples. The experimental spectra of pure CdS and CdO and their combination T (91% CdS - 9% CdO) are also included.

XANES spectra corresponding to two-phase crystal mixtures with varying mass fraction were calculated. The spectrum associated with a mixture of 91% of CdS crystals and 9% of CdO (curve T) in the way it has precipitated in the white sample (**W**) exhibits a good agreement with that of the diffused sample **M**, as can be seen in Figure 2.

The XANES results indicate that (i) the particles observed in the TEM micrograph of sample **W** are CdO nanoparticles, crystalline and/or amorphous; (ii) the nanocrystals in the diffused sample M are composed of a mixture of CdO and CdS. Theoretical calculations indicate that a volume fraction of 91 wt.% CdS and 9 wt.% CdO produce a XANES spectrum in good agreement with the experimental one.

SAXS Analysis

SAXS measurements were also performed using the DCl synchrotron radiation source at LURE (Orsay, France). The scattered intensity was recorded for every sample studied as a function of the modulus of the scattering vector q, which is related to the scattering angle ε by $q = \frac{4\pi}{\lambda}\sin(\varepsilon/2)$. The incident beam had a very small cross-section (pinhole collimation) and its wavelength was λ = 1.60 Å. The parasitic scattering from air and slits was subtracted from the total experimental scattering function.

SAXS measurements were performed for the four above-mentioned samples (**A**, **W**, **DS** and **DL**). The SAXS intensities produced by these samples were plotted in Figure 3 in the standard double logarithmic scale, the studied q-region is related with the length scale through q = π/L.

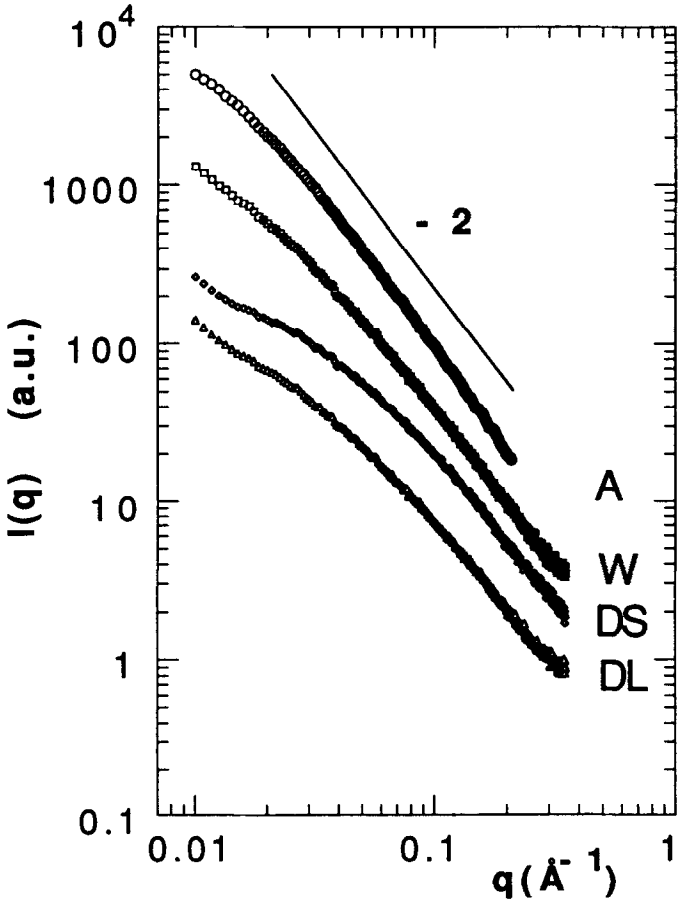

Figure 3. Log-log plots of the **A**, **W**, **DS** and **DL** SAXS intensities, from top to bottom.

The curve of sample A in Figure 3 corresponds to the wet gel without Cd, which was prepared under similar conditions to the other samples. The SAXS of this sample are produced by the electron density heterogeneities associated with the porous structure. Curve **W**, corresponding to the white sample, exhibits differences at very small q-values, when compared with curve **A**. These differences are more accentuated in the intensity curves **DS** and **DL**.

A first qualitative analysis of Figure 3, taking also into account the TEM and XANES results, suggests that the differences of curves **W**, **DS** and **DL** as compared to **A** are produced by heterogeneities due to CdO and CdS nanocrystals immersed in the silica matrix.

The analysis of SAXS results under these conditions is not straightforward, since the samples have four phases of different electronic concentration (SiO_2 skeleton, pores partially filled with liquid, CdO and CdS nanocrystals). In order to obtain useful information about structure from SAXS results, simplifying assumptions should be made.

The analysis of curve **A** suggests that the host silica gels have a structure that can be described as a fractal with dimensionality D = 1.98 that corresponds to a hierarchical reaction-limited aggregation (RLA) model. The further simplifying assumption was that the SAXS amplitude produced by the pores is not strongly correlated with that produced by CdO and CdS nanocrystals. Under this condition, we can subtract from the total scattering intensity $I_T(q)$ (curves **W**, **DS** and **DL** in Figure 3) the contribution from the pores $I_A(q)$ (curve **A**) and, thus, isolate the scattering from the small CdO and CdS crystals. Since curve **A** does not have the same scale as the others, in the subtraction

$$1_\Delta (q) = I_T (q) - K\, I_A (q) \qquad [1]$$

K was chosen in such a way that the difference curves follow Guinier's law

$$I_\Delta(q) = I(0)\, e^{-\frac{1}{3}R_G{}^2 q^2} \qquad [2]$$

over a wide q-range around the region where the bend is noticeable (0.015-0.05 $Å^{-1}$). In order to prove the reliability of our assumption, the K-values were varied until they are 4% and R_G never surpasses a 7% of the calculated values, behaving always $R_G(W) > R_G(DL) > R_G(DS)$.

In equation [2] R_G corresponds to the average gyration radius of the nanocrystals. The subtraction was performed for curves **W**, **DS** and **DL** of Figure 3. These subtractions assume that nanocrystals scatter independently and, in the case of curves **DS** and **DL**, that the differences in electronic density between crystals and SiO_2 matrix is approximately the same for CdO and CdS.

The $I_\Delta(q)$ difference curves are plotted in Figure 4 in In I(q) *vs.* q^2 scale (Guinier plot). The average gyration radius of the nanocrystals obtained from the plots of Figure 4 is 4.5, 3.2 and 3.5 nm for samples **W**, **DS** and **DL**, respectively.

Under the assumption of the simple model proposed, the SAXS results are consistent with the conclusions of TEM and XANES. CdO crystals are formed in the "white" sample with an average gyration radius of 4.5 nm. The addition of $S^=$ ions to the "white" sample shifts the average diameter to lower values (R_G = 3.2 or 3.5 nm, depending on the amount of diffused H_2S). This reduction in particle size is connected with the formation of CdS crystals from the conversion of CdO particles, because they are produced by a fast diffusion process in an environment with a lower Cd dispersion, which is already concentrated in the form of CdO particles. The reduction in

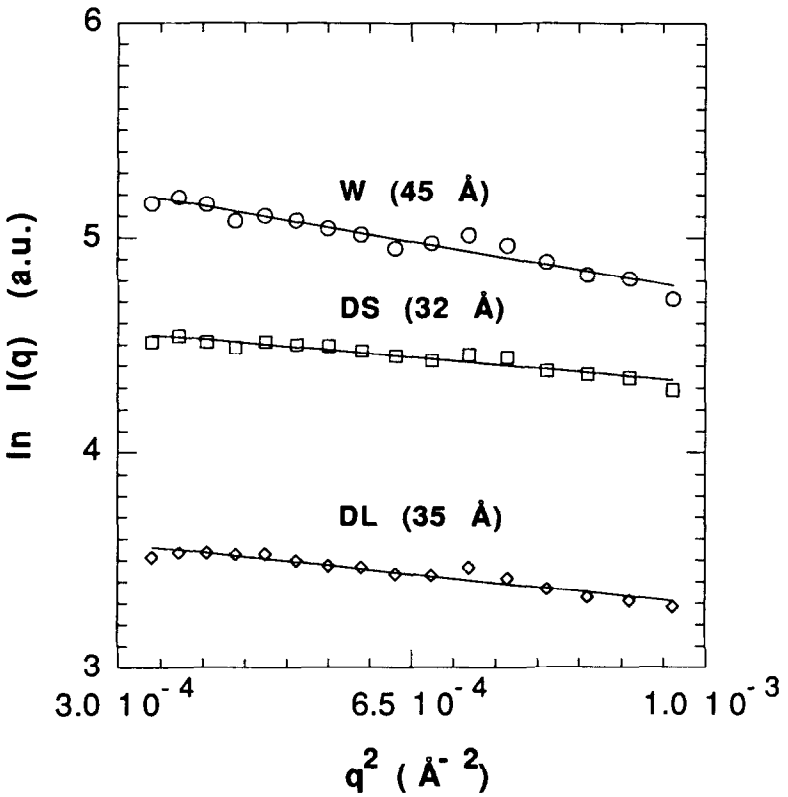

Figure 4. Guinier plots of the intensity differences for the **W**, **DS** and **DL** samples after weighted subtraction (equation [1]) of the pore-matrix contribution of the **A** sample.

average size as compared to the "white" (**W**) sample is more noticeable for samples with lower $S^=$ diffusion. As a matter of fact, the average radius is $R_G = 3.5$ nm for a sample with long time H_2S diffusion, and $R_G = 3.2$ nm for a short time H_2S diffusion.

Optical Spectrum

All diffused samples show a characteristic absorption around 420 nm wavelength (2.95 eV), blue shifted from the CdS bulk centered in 512 nm (2.42 eV). This increase in the energy to create an electron-hole pair seems to be related to excitonic quantum confinement of CdS nanocrystals embedded in the dielectric silica matrix. This effect was already reported in reference (11) and is shown in Figure 5 for **DS** doped gel composite, which is compared with the **W** sample spectrum.

CONCLUSIONS

The characterization methods (TEM, XANES) used to test the CdS-doped sonogels reveal: first, the existence of CdO particles (amorphous and/or crystalline) due to an incomplete

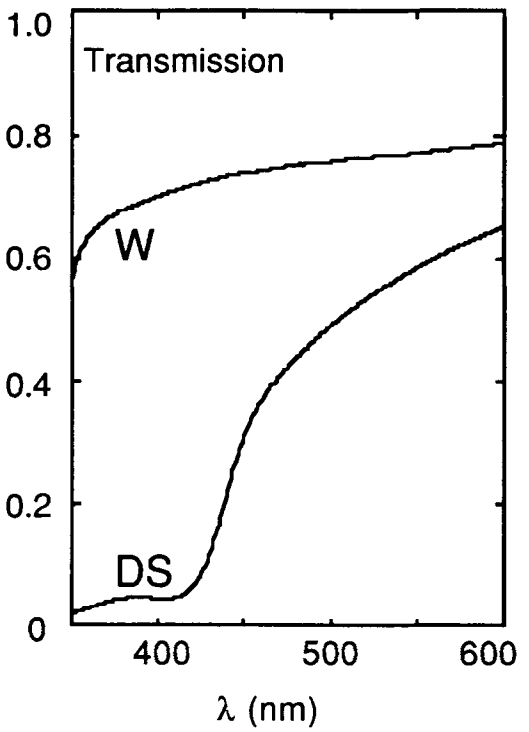

Figure 5. Room temperature UV-Vis transmission spectra of the **W** and **DS** samples.

sulphurization throughout the matrix volume. Second, the effective conversion of CdO → CdS leads to a CdS composition of 9 wt.% of the final composite SiO_2-CdS.

SAXS experiments confirmed the presence of smaller scattering entities that can be identified with CdO and CdS nanocrystals. Mathematical data reduction of the experimental intensities permitted the determination of their average size, in the range from 3 to 5 nm for the gyration radii. Therefore, the composites can be considered to have a bimodal distribution, corresponding to the remaining mesoporosity (> 10 nm) and the nanocrystals.

The nanocrystalline CdS-doped sonogels produce an absorption band in the UV-Vis spectrum at room temperature with a characteristic "blue shift", which reveals the effect of carrier confinement and the consequent non-linear optical behavior of the material.

ACKNOWLEDGEMENTS

This work was supported by the Instituto de Cooperación Iberoamericano and the project MAT91-1022 of CICYT in Spain, and the CNPq in Brazil.

REFERENCES

1. C.J. Brinker and G.W. Scherer, *Sol-Gel Science: The Physics and Chemistry of Sol-Gel Processing*, Academic Press, San Diego, CA (1990).

2. J. Zarzycki, *Glasses and the Vitreous State*, Cambridge University Press, Ch. 18 (1991).
3. *Advanced Materials from Gels*, ed. Luis Esquivias, J. Non-Cryst. Solids, 147-148 (1992).
4. R.K. Jain and R.C. Lind, J. Opt. Soc. Am. 73, 647 (1983).
5. Al.L. Éfros and A.L. Éfros, Sov. Phys. Semicond. 16 (7), 772 (1982).
6. A.I. Ekimov, Al.L. Éfros and Onushchenko, Solid State Comm. 56 (11), 921 (1985).
7. C.M. Bagnall and J. Zarzycki, J. Non-Cryst. Solids 121, 221 (1990).
8. M. Nogami and K. Nagasaka, J. Non-Cryst. Solids 122, 101 (1990).
9. T. Gacoin, C. Train, F. Chaput, J.P. Boilot, P. Aubert, M. Gandais, Y. Wang and A. Lecomte, SPIE Vol. 1758, Sol-Gel Optics 11, 565 (1992).
10. T. Takada, T. Yano, A. Yasumori, M. Yamane and J.D. Mackenzie, J. Non-Cryst. Solids 147-148, 631 (1992).
11. T. Takada, Ch-Y. Li, J.Y. Tseng and J.D. Mackenzie, J. of Sol-Gel Sci. and Tech. 1, 123 (1993).
12. J.D. Mackenzie, J. of Sol-Gel Sci. and Tech. 1, 7 (1993).
13. M. Yamane, T. Takada, J.D. Mackenzie and Ch-Y. Li, SPIE Vol. 1758, Sol-Gel Optics II, 577 (1992).
14. M. Piñero, R. Litran, C. Fernández-Lorenzo, E. Blanco, M. Ramírez-del-Solar, N. de la Rosa-Fox, L. Esquivias, A. Craievich and J. Zarzycki, J. of Sol-Gel Sci. and Tech 2 (1-3), 689 (1994).
15. E. Blanco, Ph.D. thesis, University of Cadiz (1993).
16. D. Larrue, Ph. D. thesis, University of Montpellier (1993).
17. M. Canvas, D. Larrue and J. Zarzycki, SPIE Vol. 1758, 538, Sol-Gel Optics II (1992
18. E. Blanco, R. Litrán, M. Rámirez-del-Solar, N. de la Rosa-Fox and L. Esquivias, J. Mater. Res. 9 (11), 2873 (1994).